Supplementary Information for

Transient Structures and Possible Limits of Data Recording in Phase-Change Materials

Jianbo Hu, Giovanni M. Vanacore, Zhe Yang[†], *Xiangshui Miao*[†] and *Ahmed H. Zewail**

Affiliations:

Physical Biology Center for Ultrafast Science and Technology, Arthur Amos Noyes Laboratory of Chemical Physics, California Institute of Technology, Pasadena, CA 91125, USA

*To whom correspondence should be addressed. E-mail: zewail@caltech.edu

†Permanent address: Wuhan National Laboratory for Optoelectronics, Huazhong University of Science and Technology, Wuhan 430074, China

Laser crystallization of GeTe film

To obtain crystalline GeTe samples from the as-deposited amorphous films, two different methods have been explored: i) static thermal annealing, and ii) femtosecond laser annealing. For the static annealing, a tube furnace at relatively low vacuum has been used with a temperature of 350 °C for 10 min, as described in details in the methods section of the main text. For the laser annealing, crystallization was reached under 120 fs infrared (800 nm) pulses at 1 KHz repetition rate and fluence of 6.7 mJ/cm^2 for 2 hours. The diffraction patterns obtained in the two cases, shown in Fig. S1, exhibit similar features and are representative of the rhombohedral α phase, attesting to the relevance of local distortions of the cubic symmetry in all laser-based technological applications. It is also important to mention that the time dependence of the peak intensity change observed for the GeTe samples made by static annealing, shown in Fig. 5c in the main text, were also observed in the case of laser-annealed films.

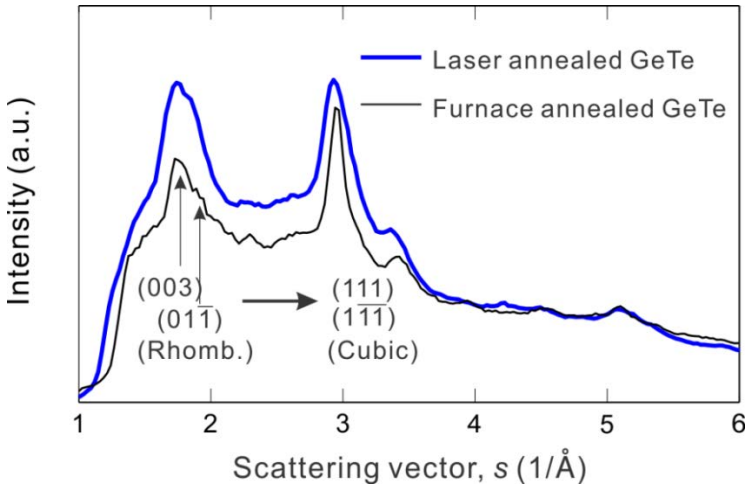

Fig. S1. Diffraction patterns obtained by femtosecond laser annealing (blue line) and static thermal annealing (black line). The two indexed peaks correspond to (003) and (01$\bar{1}$) reflections in the rhombohedral phase, which can be transformed into (111) and (1$\bar{1}\bar{1}$) peaks in cubic system. In perfect cubic symmetry the two peaks would have the same scattering vector; the clear observation of a splitting in the reciprocal space between them is consistent with the existence of local lattice distortions associated with the rhombohedral structure.

Rate equations model

In crystalline GeTe the α-to-β transition is mediated by the instability caused by both the electronic and structural states.[1] Two coupled sub-systems are involved, one that relates to the electronic change of the interatomic potential and the other which is driven by the deformation of the unit cell.

The mechanism behind the transformation from a rhombohedral to a cubic phase has already been described in the main text. Briefly, when the photo-excited carrier density reaches a threshold value, a movement of Te atoms takes place and changes the interatomic potential from a double to a single well. This is a displacive excitation and occurs in a sub-picosecond time scale.[2-4] A shear structural deformation of the unit cell is necessary to complete the transition, whose time scale is determined by the excitation of acoustic phonons *via* anharmonic decay of optical phonons; at room temperature it occurs in 12 ps.[5]

These changes are expressed in the following rate equations model:

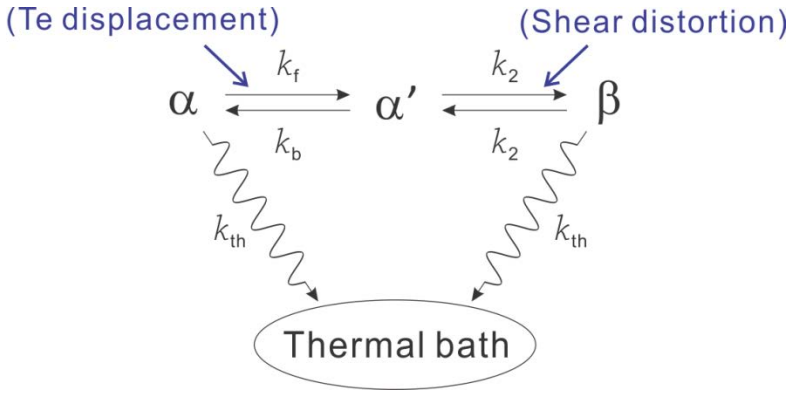

Fig. S2. Kinetic processes involved in the phase change of crystalline GeTe. k_f and k_b are, respectively, the rate constants for $\alpha \rightarrow \alpha'$ and $\alpha' \rightarrow \alpha$ transitions, which are defined by the displacement of Te atoms; k_2 is the rate constant for the $\alpha' \rightleftharpoons \beta$ transition mediated by the shear distortion; and k_{th} is the rate constant for reaching the thermal equilibrium.

The kinetics of the transition can be described as shown in Fig. S2, assuming a reversible and sequential transformation from α to β. Here α' indicates the structural state of the lattice following the Te atom movement to the center, but prior to the shear deformation (see also Fig. 2 in the main text). The rate equations can be written as:

$$\frac{dP_{\alpha'}}{dt} = k_f P_\alpha + k_2 P_\beta - k_b P_{\alpha'} - k_2 P_{\alpha'} \qquad \text{for the } \alpha' \text{ phase} \tag{S1}$$

$$\frac{dP_\beta}{dt} = k_2 P_{\alpha'} - k_2 P_\beta \qquad \text{for the } \beta \text{ phase} \tag{S2}$$

where P is the transition probability; the subscripts 'α', 'α'' and 'β' represent the three structural states; k_f and k_b are the carrier density-dependent rate constants for $\alpha \to \alpha'$ and $\alpha' \to \alpha$ transitions, respectively; and k_2 is the rate constant for the $\alpha' \rightleftharpoons \beta$ transition, which depends on the excitation of acoustic phonons.

Since the formation of the α'-phase is mediated by the coupling between electrons and optical phonons, it typically occurs on a sub-picosecond time scale.[3] This means that k_f and k_b are much larger than k_2. From equation S1, we thus obtain that $P_{\alpha'}$ exhibits a step-like behavior as a function of the excited carrier density, N_e, which is consistent with the picture where the phase transition is triggered only when N_e reaches a threshold value. Within this context, the transition probability P_β can be then calculated using the equation S2. The change of the rhombohedral angle is taken to vary linearly with P_β.

The dynamics of the photo-excited carriers is given by:

$$\frac{dN_e}{dt} = Q_{laser} - \frac{N_e}{\tau_t} - CN_e^3 \tag{S3}$$

where τ_t is the time constant of carrier trapping by defects, CN_e^3 describes the carrier recombination by Auger processes,[6] and $Q_{laser} = S_{laser}/h\nu$ is the density of absorbed photons. Here, the photon energy $h\nu$ is 1.55 eV, and $S_{laser} = \frac{0.94F_{laser}}{t_p \cdot \delta}(1-R_{laser})\exp\left[-2.77\left(\frac{t}{t_p}\right)^2 - \frac{z}{\delta}\right]$ represents the laser source, where F_{laser} is the incident fluence, t_p the pulse duration, R_{laser} the reflectivity, and δ the penetration depth (1/*e*). Because of the low electron mobility,[7] the charge carrier diffusion has been neglected. For α-GeTe, R_{laser} = 0.4858 and δ = 14 nm at the wavelength of 800 nm, as derived from the measured dielectric function given in Ref. 8. No experimental or theoretical values for τ_t and C are reported in the literature, and thus they have been adjusted to reach the best matching between experiments and simulations.

Because the penetration depth for the excitation pulse at 800 nm in α-GeTe is 14 nm (1/*e*), smaller than the film thickness, we expect that only within the top few nanometers of the film the excited carrier density will reach the threshold value to drive the transition toward the β phase, see Fig. S3. Following the excitation, heat transfer will take place within the sample thickness reaching the thermal equilibrium in hundreds of picoseconds.

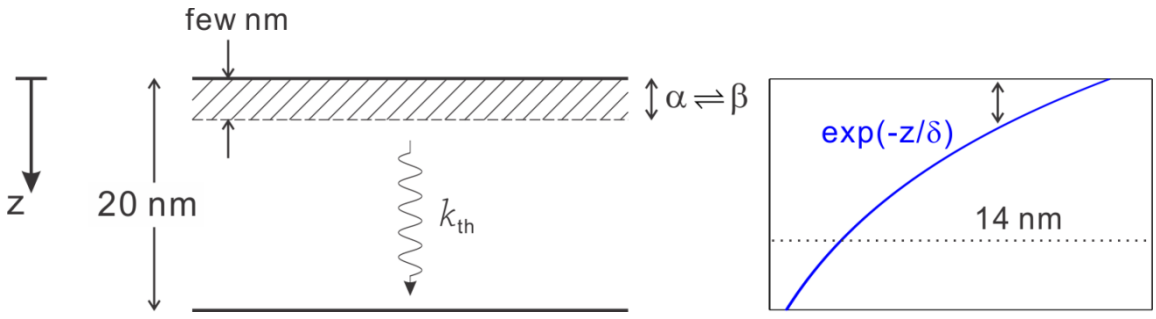

Fig. S3. Schematic representation of the excitation process in a GeTe nano-film. The transition to the β phase takes place only within the top region. A thermal equilibrium occurs with a rate constant k_{th}, given by the heat diffusion within the sample thickness.

Modified two-temperature model

The energy transfer toward the lattice following the ultrafast optical excitation can be described within the framework of the two-temperature model (TTM),[9] in which the electron and lattice subsystems are assumed to reach a local equilibrium and that their energy state is defined by the temperatures $T_e(z,t)$ and $T_l(z,t)$, respectively. Because GeTe has two atoms per unit cell in the rhombohedral α-phase, an intermediate process involving the excitation and decay of optical phonons occurs during the energy transfer from electrons to acoustic phonons. However, this process will not affect the temperature distribution in the final state and, for the purposes of the current analysis, can be neglected. However, the redistribution of the energy accumulated within the β-phase toward the thermal bath has to be explicitly taken into account (see Fig. S2). This is obtained by including the rate of the transition probability for the β phase, dP_β/dt, within the equations describing the TTM, which can be written as:

$$C_l \frac{\partial T_l}{\partial t} = \nabla \cdot \left(K_l \nabla T_l\right) + \frac{C_e}{\tau_e}\left(T_e - T_l\right) + \frac{dP_\beta}{dt} \cdot F_{abs} \tag{S4}$$

$$C_e \frac{\partial T_e}{\partial t} = \nabla \cdot \left(K_e \nabla T_e\right) - \frac{C_e}{\tau_e}\left(T_e - T_l\right) + S_{laser} - \frac{dP_\beta}{dt} \cdot F_{abs} \tag{S5}$$

where C_e and C_l are the heat capacities of the electron and lattice subsystems, respectively; K_e and K_l are the thermal conductivity of the two subsystems; $\tau_e = 10$ ps, the coupling time between electrons and lattice and is estimated from the anharmonic decay constant of the optical phonons;[5] and $F_{abs} = F_{laser} \cdot \left(1 - R_{laser}\right)/\delta$ is the absorbed fluence. For GeTe, $C_l = (1.49 \times 10^6 + 3.88 \times 10^2 \cdot T_l)$ $J/(m^3 \cdot K)$, $C_e = (85.4 \cdot T_e)$ $J/(m^3 \cdot K)$, $K_l = 4.184$ $W/(m \cdot K)$, and $K_e = 1.3$ $W/(m \cdot K)$, as derived from Ref. 10 and 11.

The simulations reproduce all major features of the experimental data and their dependence on the delay time and excitation fluence. As for the estimation of the temperature, it is worth mentioning that the possible effect of the latent heat associated with the phase transition, and the contribution of the radiative recombination of the charge carriers have not been considered, and because of this the temperatures calculated within the TTM model described above over-estimates the real values, as also observed in recent time-resolved x-ray diffraction studies.[12] Nevertheless, a correct estimation of the lattice temperature can be reliably obtained from the intensity and peak-position data at long delay time (~ 400 ps), as shown in the main text in Figs. 3b and 3d.

Transient change of diffraction intensity and peak position

The intensity of the (hkl) Bragg reflection, I_{hkl}, is proportional to the square modulus of the structure factor, $F_{hkl}(\mathbf{r}) = \sum_j f_j \exp\left[-2\pi i (hkl)\cdot \mathbf{r}_j\right]$, where $\mathbf{r}_j$ is the position of the *j*th atom and (hkl) is the scattering vector. The intensity change associated with the α-to-β transition can be calculated as a linear combination of the square modulus of the structure factors for the two phases, $F(\mathbf{r}^\alpha)$ and $F(\mathbf{r}^\beta)$, where the weights are given by the probabilities P_β and $P_\alpha = (1 - P_\beta)$:

$$\frac{I_{nth}}{I_\alpha} \propto \left(1 - P_\beta(z,t)\right) + \frac{\left|F(\mathbf{r}^\beta)\right|^2}{\left|F(\mathbf{r}^\alpha)\right|^2} \cdot P_\beta(z,t) \qquad \text{(S6)}$$

Here, $\mathbf{r}^\alpha$ and $\mathbf{r}^\beta$ are the positions of the Ge atoms in the α and β phases, respectively (see Fig. 2 in the main text); the Te atoms are considered to occupy the cubic lattice sites.[13]

In Fig. S4, we present the results of the simulations for the observed Bragg reflections. The increase of the intensity for the (220) peak is consistent with the 'allowed' nature of this reflection in the cubic β-phase, whereas the decrease for the (111) and (113) peaks well correlates with their 'quasi-forbidden' character in a cubic structure. The recovery toward the equilibrium condition, i.e. the initial α-phase, is mediated by nonradiative carrier recombination occurring in hundreds of ps in GeTe, and it is the origin of system relaxation toward its initial equilibrium state.

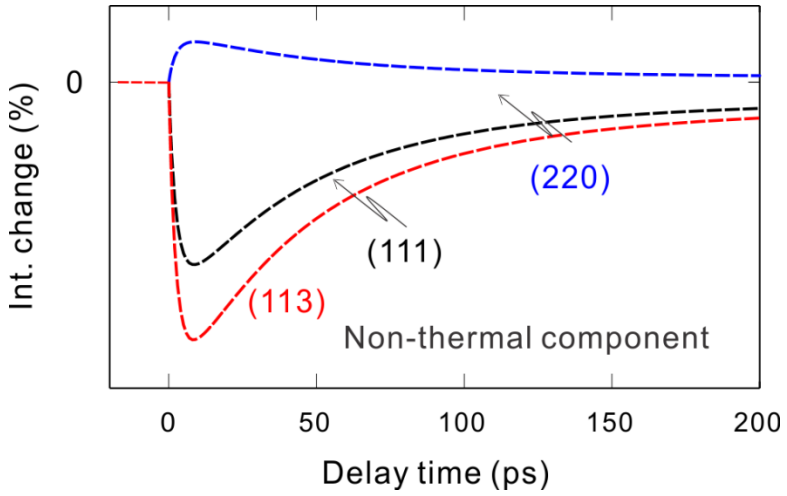

Fig. S4. Simulated temporal change of the structure factors for three observed Bragg reflections associated with the α-to-β transition. Thermal effects are not included in this figure, but considered in the text.

Besides the structural change induced by the phase transition, the intensity is also affected by the thermal heating of the lattice, which is described by the Debye-Waller effect. The total intensity change is thus expressed as:

$$\frac{I_{total}}{I_0} = \frac{I_{nth}}{I_\alpha} \exp\left[2s^2 \left(\frac{\langle u^2(T_0) \rangle - \langle u^2(T_l) \rangle}{4} \right) \right] \quad \text{(S7)}$$

where $\left\langle u^2(T)\right\rangle$ is the atomic mean-square displacement, calculated using the approach presented in Ref. 14:

$$\left\langle u^2(T)\right\rangle = \frac{3\hbar^2}{2mk_b\theta_D}\left[1+4\left(\frac{T}{\theta_D}\right)^2\int_0^{\theta_D/T}\frac{x}{\exp(x)-1}dx\right] \quad \text{(S8)}$$

Here, m is the average mass within a GeTe basis, k_b is the Boltzmann constant, and θ_D = 180 K is the Debye temperature for α-GeTe.[15] Since the experiments are performed in the transmission geometry, the observed dynamics is determined by the averaged contribution along the direction of electron beam. Therefore, a direct comparison with the experimental results can be done only by averaging the calculated intensity change I_{total}/I_0 over the whole sample thickness.

The position change of the diffraction peaks is due to the combined effect of the shear deformation of the unit cell and the thermal expansion. The variation of the scattering vector, *s*, can thus be expressed as:

$$\Delta s = s_0 \cdot \left(P_\beta(t)\cdot\varepsilon^0 + \alpha_{th}\cdot\Delta T(t)\right) \quad \text{(S9)}$$

where α_{th} =1.9×10^{-5} K^{-1} is the linear thermal expansion coefficient,[16] and ε^0 is the uniaxial shear strain necessary to increase the rhombohedral angle from 57.94° to 60°, assuming a rigid angle change and no variation of the bond length within the unit cell. In equation S9, ΔT represents the temperature rise due to laser heating and is given by a single-exponential increase with a time constant given by $1/k_{th} = \tau_{th} = l^2/D$ (l is the film thickness, $D = K_l/(\rho\cdot C_l)$ is the heat diffusion coefficient, and ρ is the mass density), and a total temperature jump as experimentally derived from the slow component of the intensity change (see Fig. 3b in the main text). The calculated change for the (220) peak is shown in Fig. 5b of the main text.

Anisotropic shear strain

As described in the main text, the completion of the α-to-β transition corresponds to the increase of the rhombohedral angle, φ, from 57.94° to 60°. As mentioned above, the shear motion responsible for the angle change can be decomposed along the [111] and [$00\bar{1}$] directions. From the measured change of the peak-position for the (220), (111) and (113) reflections, we determined the lattice strains, $\varepsilon_{(220)} = (\Delta s/s)_{(220)}$, $\varepsilon_{(111)} = (\Delta s/s)_{(111)}$, and $\varepsilon_{(113)} = (\Delta s/s)_{(113)}$, along the corresponding directions. At each fluence, the strain components, $\varepsilon^s_{(111)}$ and $\varepsilon^s_{(00\bar{1})}$ along the [111] and [$00\bar{1}$] directions, can be obtained by projecting the measured deformations, $\varepsilon_{(220)}$, $\varepsilon_{(111)}$, and $\varepsilon_{(113)}$ along those directions. In Fig. S5a, we plot the obtained fluence dependence. The observation of larger values for $\varepsilon^s_{(00\bar{1})}$ than those obtained for $\varepsilon^s_{(111)}$ is consistent with an increase of the rhombohedral angle toward the cubic symmetry.

With simple geometric considerations, it is also straightforward to calculate the value of $\varepsilon^0_{(111)}$ and $\varepsilon^0_{(00\bar{1})}$ to reach the condition φ = 60°, with a simultaneous isotropic contraction of 0.28 % of the bond length.[1] These are 0.6×10^{-2} and 1.2×10^{-2}, respectively. As discussed above, considering that the penetration depth for the excitation pulse at 800 nm in α-GeTe is 14 nm (1/*e*), smaller than the film thickness, only the top few nanometers of the film have excited carrier density that will reach the threshold value necessary to trigger the transition to the β phase. Using the kinetic model described above, we determine that only a percentage P_β of the unit cells are transformed. The effective strains can thus be obtained: $\varepsilon^s_{(hkl)} = \varepsilon^0_{(hkl)} \cdot P_\beta$, which are shown in Fig. S5b as a function of the fluence. The results are in good agreement with the experimental observations displayed in Fig. S5a (see text).

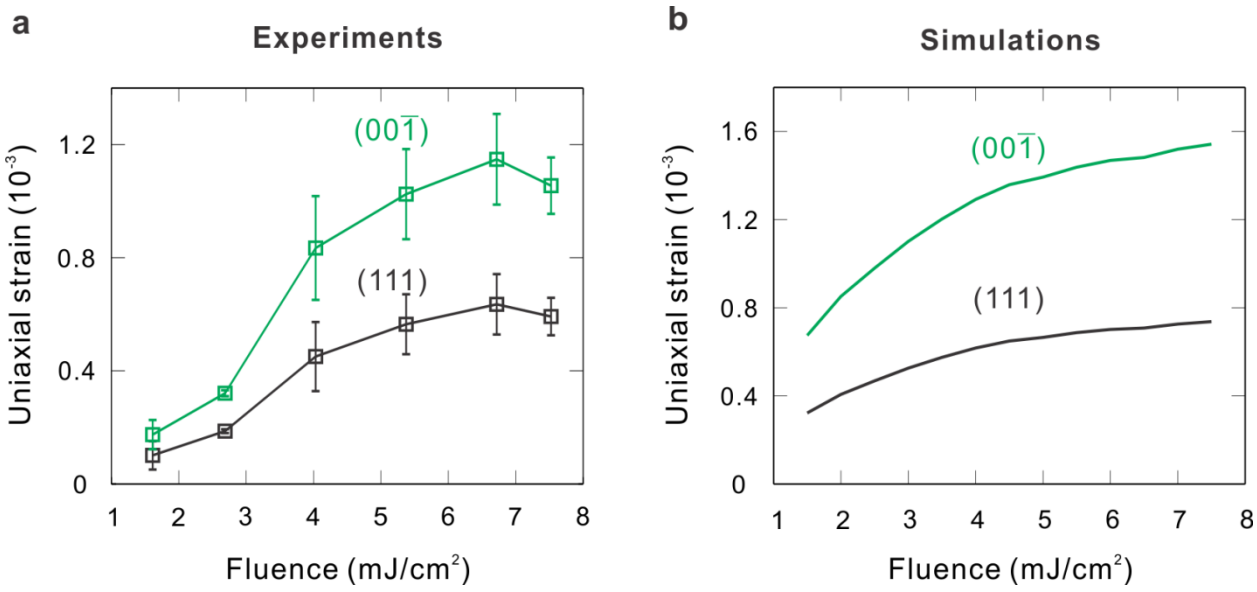

Fig. S5. Experimental (**a**) and calculated (**b**) lattice strains along the [111] and [$00\bar{1}$] directions, induced by the shear motion (increase of rhombohedral angle) and isotropic bond length contraction within the GeTe unit cell. Shown is the behavior as a function of the fluence.

REFERENCES

1 Chattopadhyay, T.; Boucherle, J. X.; Vonschnering, H. G. Neutron Diffraction Study on the Structural Phase Transition in GeTe. *J. Phys. C-Solid State* **1987,** *20*, 1431-1440.

2 Fritz, D. M.; Reis, D. A.; Adams, B.; Akre, R. A.; Arthur, J.; Blome, C.; Bucksbaum, P. H.; Cavalieri, A. L.; Engemann, S.; Fahy, S. *et al.* Ultrafast Bond Softening in Bismuth: Mapping a Solid's Interatomic Potential with X-rays. *Science* **2007,** *315*, 633-636.

3 Sciaini, G.; Harb, M.; Kruglik, S. G.; Payer, T.; Hebeisen, C. T.; Heringdorf, F. J. M. Z.; Yamaguchi, M.; Hoegen, M. H. V.; Ernstorfer, R.; Miller, R. J. D. Electronic Acceleration of Atomic Motions and Disordering in Bismuth. *Nature* **2009,** *458*, 56-60.

4 Murray, E. D.; Fritz, D. M.; Wahlstrand, J. K.; Fahy, S.; Reis, D. A. Effect of Lattice Anharmonicity on High-Amplitude Phonon Dynamics in Photoexcited Bismuth. *Phys. Rev. B* **2005,** *72*, 060301.

5 Hase, M.; Miyamoto, Y.; Tominaga, J. Ultrafast Dephasing of Coherent Optical Phonons in Atomically Controlled GeTe/Sb_2Te_3 Superlattices. *Phys. Rev. B* **2009,** *79*, 174112.

6 Sundaram, S. K.; Mazur, E. Inducing and Probing Non-Thermal Transitions in Semiconductors Using Femtosecond Laser Pulses. *Nature Mater.* **2002,** *1*, 217-224.

7 Lyeo, H. K.; Cahill, D. G.; Lee, B. S.; Abelson, J. R.; Kwon, M. H.; Kim, K. B.; Bishop, S. G.; Cheong, B. K. Thermal Conductivity of Phase-Change Material $Ge_2Sb_2Te_5$. *Appl. Phys. Lett.* **2006,** *89*, 151904.

8 Shportko, K.; Kremers, S.; Woda, M.; Lencer, D.; Robertson, J.; Wuttig, M. Resonant Bonding in Crystalline Phase-Change Materials. *Nature Mater.* **2008,** *7*, 653-658.

9 Anisimov, S. I.; Kapeliovich, B. L.; Perel'man, T. L. Electron Emission from Metal Surface Exposed to Ultrashort Laser Pulses. *Sov. Phys. -JETP* **1974,** *39*, 375-377.

10 Mills, K. C. *Thermodynamic Data for Inorganic Sulphides, Selenides and Tellurides*. Butterworth-Heinemann: London, 1974.

11 Nath, P.; Chopra, K. L. Therma Conductivity of Amorphous and Crystalline Ge and GeTe Films. *Phys. Rev. B* **1974,** *10*, 3412-3418.

12 Fons, P.; Rodenbach, P.; Mitrofanov, K. V.; Kolobov, A. V.; Tominaga, J.; Shayduk, R.; Giussani, A.; Calarco, R.; Hanke, M.; Riechert, H. *et al.* Picosecond Strain Dynamics in $Ge_2Sb_2Te_5$ Monitored by Time-Resolved X-ray Diffraction. *Phys. Rev. B* **2014,** *90*, 094305.

13 Biquard, X.; Krbal, M.; Kolobov, A. V.; Fons, P.; Simpson, R. E.; Hyot, B.; Andre, B.; Tominaga, J.; Uruga, T. Effect of Doping on Global and Local Order in Crystalline GeTe. *Appl. Phys. Lett.* **2011,** *98*, 231907.

14 Schafer, S.; Liang, W. X.; Zewail, A. H. Primary Structural Dynamics in Graphite. *New J. Phys.* **2011,** *13*, 063030.

15 Pereira, P. B.; Sergueev, I.; Gorsse, S.; Dadda, J.; Muller, E.; Hermann, R. P. Lattice Dynamics and Structure of GeTe, SnTe and PbTe. *Phys. Status Solidi B* **2013,** *250*, 1300-1307.

16 Wiedemeier, H.; Siemers, P. A. Thermal Expansion of GeS and GeTe. *Z. Anorg. Allg. Chem.* **1977,** *431*, 299-304.